

Interfacial Stereoelectronic Effect Induced by Anchoring Orientation

Xiao Wei,[▽] Jinying Wang,[▽] Xinyue Chang, Suhang He, Ping Duan,* Chuancheng Jia,* and Xuefeng Guo*Cite This: *Nano Lett.* 2024, 24, 9399–9405

Read Online

ACCESS |



Metrics & More



Article Recommendations



Supporting Information

ABSTRACT: Heterogeneous interfaces in most devices play a key role in the material performance. Exploring the atomic structure and electronic properties of metal–molecule interfaces is critical for various potential applications, such as surface sensing, molecular recognition, and molecular electronic devices. This study unveils a ubiquitous interfacial stereoelectronic effect in conjugated molecular junctions by combining first-principles simulation and scanning tunneling microscopy break junction technology. Single-molecule junctions with same-side interfacial anchoring (*cis* configuration) exhibit higher conductance than those with opposite-side interfacial anchoring (*trans* configuration). The *cis* and *trans* configurations can undergo reversible conversions, resulting in a conductance switching. The stability of these configurations can be adjusted by an electric field, achieving precise regulation of conductance states. Our findings provide important insights for designing high-quality materials and enhancing the device performance.



KEYWORDS: interfacial stereoelectronic effect, single-molecule junction, anchoring orientation, charge transport

Material interfaces featuring distinct chemical and physical properties exert a profound influence on the behavior and functionality of diverse devices.^{1–4} For instance, in semiconductor device engineering, interface manipulation is crucial for enhancing the device performance such as charge carrier mobility,⁵ heat- and charge-transfer efficiency,⁶ light absorption and charge separation,⁷ mechanical integrity and durability,⁸ chemical reactivity,⁹ and more. In the realms of biology and medicine, interfaces are indispensable for the biological processes¹⁰ like cell adhesion,¹¹ drug delivery,¹² and biomaterial compatibility.¹³ In particular, the metal–molecule interface¹⁴ plays a critical role not only in established scientific disciplines like surface chemistry and micro/nanoelectronics, but also in cutting-edge research fields such as quantum computing¹⁵ and molecular electronics.¹⁶ In general, organic molecules are connected to metal surfaces through both covalent and noncovalent bonds, such as metal–S¹⁷ and metal–C¹⁸ σ bonds or metal– π ¹⁹ and metal–NH₂²⁰ noncovalent interactions. These intricate interfacial interactions exercise precise control over the structural, chemical, and electronic properties of metal–molecule interfaces, ultimately shaping the performance of molecular devices.

Single-molecule junction techniques, such as mechanical break junctions,^{21,22} electrical breakdown junctions,^{23,24} and lithography-defined junctions,^{25,26} can be used to characterize the intrinsic physical and chemical properties of both molecules²⁷ and metal–molecule interfaces.²⁸ In particular, the charge transport characteristics through the interface between a single molecule and electrodes have been extensively studied, which provides critical insights into the structural transformations, charge dynamics, and alterations in electronic states.^{29,30} Stereoelectronic effects that refer to the conductance switching due to stereoisomerism of device

configurations have been intensively studied in recent years. Previous studies^{31–33} on stereoelectronic effects have mainly focused on the molecular skeleton. For instance, the stereoelectronic effect between the strong σ conjugation of the oligosilane backbone and the σ -bond of –SCH₃ has been confirmed through effectively manipulating the electrode spacing.³¹ The stereoelectronic effects of aromatic chains due to phenyl twisting have also been observed through stochastic conductance switching in single-molecule junctions.³² However, research about stereoelectronic effects of the metal–molecule interface, which is expected to be significant, is still missing.

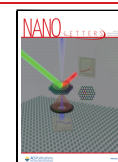
In order to differentiate the stereoelectronic effect arising from metal–molecule interfaces from that originating solely from the molecules, it is imperative to employ a molecular junction with a rigid molecular skeleton and variable interfaces. Therefore, we choose amine as a representative anchor group to link diphenylacetylene—a structurally rigid and planar molecule, to gold electrodes and attach it from different sides to create p – π conjugated molecular junctions. In this study, we combine scanning tunneling microscope break junctions (STM–BJs) technology and first-principles simulations to explore the interfacial stereoelectronic effect within these p – π conjugated molecular junctions.

Received: June 6, 2024

Revised: July 13, 2024

Accepted: July 15, 2024

Published: July 17, 2024



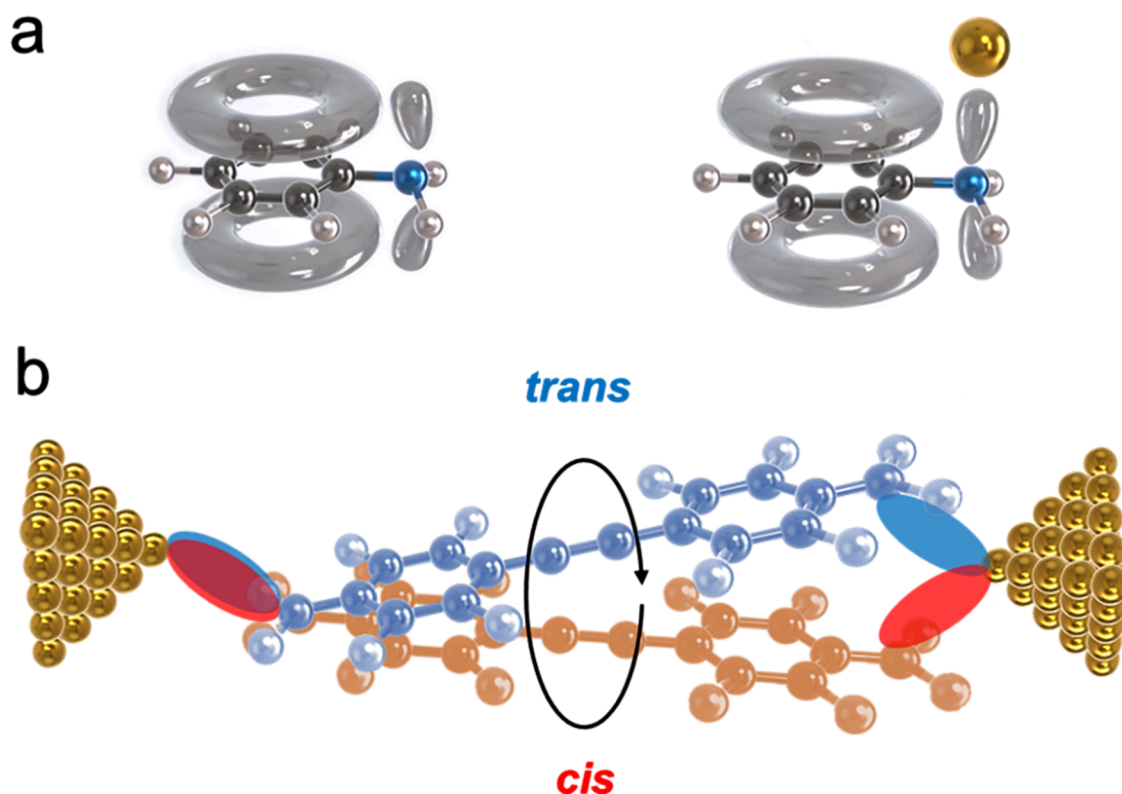


Figure 1. Stereoelectronic structures of aniline-based molecules before and after bonding with gold atoms. (a) Schematic diagram of p- π conjugated electronic structure before (left) and after (right) aniline bonding to gold atoms. (b) Schematic illustration of the interfacial anchoring of an 4,4'-ethynylenebis(benzenamine) (M1) molecule with gold atoms on the same-side (*cis* configuration) and opposite-sides (*trans* configuration), respectively.

Aniline is typically recognized for its characteristic p- π conjugated planar structure, primarily due to the substantial overlap between the p-orbital of the nitrogen atom and the delocalized π electron system within the benzene ring plane. Here, aniline is predicted to retain its atomic structure before (left) and after (right) bonding with gold atoms (Figure 1a). Specifically, a dihedral angle of $\sim 26^\circ$ between $-\text{NH}_2$ and the benzene ring in aniline remains almost the same ($\sim 24^\circ$) after aniline is connected with gold atoms, resulting in little impact on the orbital characteristics within aniline (see the orbital decomposition in Figure S1 and the C-N σ -bond analysis in eqs 1 and 2). Since previous studies^{34,35} show that the stereoelectronic effects in molecular devices primarily arise from changes in molecular structure and orbital characteristics, it is expected that there would be no discernible stereoelectronic effect within aniline-gold devices. However, the presence of direction-dependent bonding between aniline and gold introduces two distinct stereoelectronic structures in their junctions. Taking the M1 molecule (4,4'-ethynylenebis(benzenamine)) as an example, when the amino groups at both ends of the p- π conjugate molecule are connected to the gold atoms in the same direction (same-side anchoring mode), it results in a *cis* configuration; in contrast, when the amino groups at both ends are linked to the gold atoms in opposite directions (opposite-side anchoring mode), it leads to a *trans* configuration (Figure 1b). These different interfacial stereoelectronic structures, achieved through either same-side or opposite-side anchoring in molecular junctions, are anticipated to yield distinct charge-transport properties.

To explore the interfacial stereoelectronic effect, we first simulate the electronic states of Au-M1 contacts with *cis* and

trans configurations. Although the distribution of frontier orbitals within the M1 region remains nearly identical for *cis* and *trans* configurations, significant differences of the orbital distribution emerge near Au-NH₂ interfaces (see Figure 2a and Figure S2 for Au-M1 orbitals and Figure S3 for a comparison of M1 orbitals without a Au connection). The *cis* configuration is predicted to exhibit ~ 1 order of magnitude higher conductance than the *trans* configuration at the Fermi level (Figure 2b), primarily attributable to the shifts in the transmission peaks of corresponding molecular orbitals (see molecular projected self-consistent Hamiltonian (MPSH) analysis in Figure S4) due to the different Au-N distances (Figure S5) in the two configurations, as indicated by our measurements.

To validate the predicted stereoelectronic effect, we conduct the charge transport measurements on dynamic single-molecule junctions based on M1, employing a STM-BJ technology (Figure 2c). At room temperature, single-molecule conductance is measured within a dodecane mixture containing 0.1 mM M1, with the conductance being a function of tip-substrate displacement. Figure 2d displays typical individual traces for M1 junctions under a 0.1 V bias. In these traces, one can observe integer multiples of quantum conductance G_0 ($G_0 = 2e^2/h$), as well as features occurring below G_0 at specific molecular values. The black traces represent the tunneling decay after the rupture of the gold contact within the pure solvent. In contrast, when M1 is introduced into the solution, conductance plateaus corresponding to molecular conductance become evident in the red, blue, and purple traces. These representative traces signify high conductance, low conductance, and simultaneously coexisting

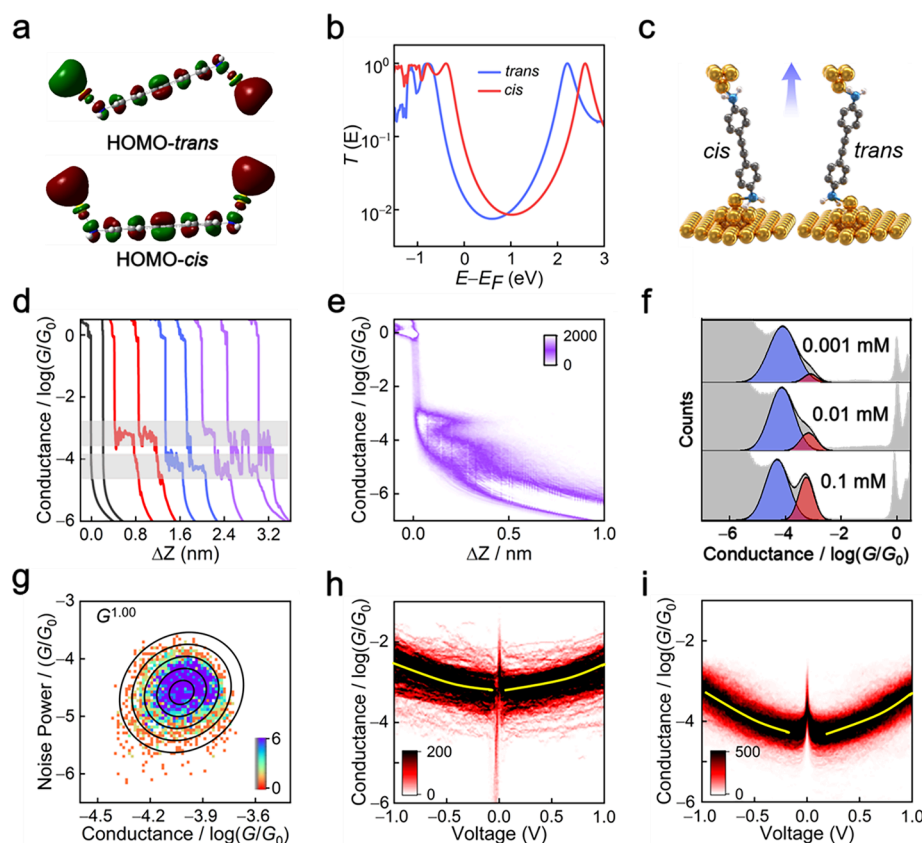


Figure 2. Single-molecule charge transport properties of M1 junctions. (a) Calculated HOMO diagrams for *trans* and *cis* conformations. (b) Calculated transmission spectra of *cis* and *trans* junctions. (c) Schematic of STM–BJ measurements. The arrow indicates the direction in which the gold tip moves. (d) Experimental conductance–displacement traces of the M1 junction at 0.1 V bias (red, blue, and purple traces) and those of Au contacts in the pure solvent (black traces). (e) 2D conductance–displacement histogram for M1 junctions. (f) 1D conductance histogram of M1 at 0.1 V and concentrations of 0.1 mM, 0.01 mM, and 0.001 mM. (g) 2D histograms of normalized flicker noise power versus average conductance for M1 junctions corresponding to low conductance state. (h, i) 2D G – V histograms of high-conductance (panel (h)) and low-conductance (panel (i)) states.

conductance plateaus, respectively. About 4000 of such conductance traces are employed to generate the conductance histograms in Figure 2e, which clearly shows the two distinct conductance states. These states are attributed to the *cis* and *trans* configurations for the following reasons. First, Gaussian-fitted conductance peaks are evident at $\sim 0.56 \times 10^{-3} G_0$ (~ 43.08 nS) and $0.5 \times 10^{-4} G_0$ (~ 3.88 nS). This nearly 1 order of magnitude difference in conductance closely aligns with our calculated transmission results. Second, the concentration-dependent measurements (see Figure 2f, as well as Figure S6) reveal that, as the concentration decreases, the conductance values of the two states do not change, but the proportion of high conductance state to low conductance state decreases. This may be due to the energy or stability difference in the *cis* and *trans* configurations. Third, charge transport in different configurations is strongly influenced by interfacial coupling, both through bonds and through space, which can be assessed using flicker noise analysis. Flicker noise analysis of M1 junctions indicates that the noise power scales of the high and low conductance states are $G^{1.00}$ and $G^{1.15}$ (see Figure 2g, as well as Figure S7), respectively, indicating that charge transport through the junction is predominantly through-bond.³⁶ Our concentration-dependent measurements and flicker noise analysis have conclusively ruled out the possibility that the low conductance states are caused by π – π stacking³⁷ of molecules. Furthermore, we also discounted the

origins of the two conductance states from molecular impurities or electrode structures. Although M1 molecules have various configurations, the *cis* and *trans* configurations considering Au–N contacts are predicted to be stable around room temperature. All the above results and analysis provide robust support for the high and low conductance states originating from the interfacial stereoelectronic effect within M1-based devices, corresponding to the *cis* and *trans* configurations, respectively. To be noted, some previous STM conductance measurements of this molecule in a mixture of 1,3,5-dimethylbenzene and tetrahydrofuran (TMB/THF) solvent have been also carried out to detect the two conductance states, but without further analysis of the mechanism.^{38,39} In contrast, only one conductance state can be observed in M1 junctions within a moderately polar solvent 1,2,4-trichlorobenzene (TCB).⁴⁰ It can be speculated that the choice of solvent plays a critical role in the observation of the two conductance states. Therefore, we conducted the same experiment using the polar solvent propylene carbonate (PC), and only a single conductance state is found (Figure S8). This suggests a solvent effect on the *cis*–*trans* configuration transition.

To gain a deeper understanding of the charge transport properties in single molecule junctions, we investigate the current–voltage (I – V) and conductance–voltage (G – V) characteristics. Specifically, the I – V characterizations are

conducted by holding the gold tip at the corresponding conductance plateau during the junction breaking measurements and scanning the bias voltage from -1.0 V to 1.0 V with a step of 0.5 mV. The collected I - V traces are used to construct 2D I - V histograms, which clearly displays the high- and low-current states (Figure S9). As shown in the 2D G - V histograms (Figure 2h and 2i), the conductance values of the two states align with the data in Figure 2e when the bias voltage remains small. As the bias voltage increases, the conductance values of both states in the M1 junctions also rise. Interestingly, the conductance growth rate for the high-conductance (*cis*) state transitions from rapid to gradual, while the low-conductance (*trans*) state experiences the reverse, shifting from gradual to rapid. This phenomenon can be attributed to the proximity of the highest occupied molecular orbital (HOMO) of the *cis* configuration to the Fermi level, compared to that of the *trans* configuration, causing the frontier orbital to enter the bias window earlier than the latter.

To further explore the transition dynamics between the *cis* and *trans* configurations of Au-M1 junctions, hovering tests are employed to investigate the conductance changes over time. During the hover mode, the length of the molecular junction remains fixed, and the Au tip ceases its back-and-forth motion. Specifically, when the electrodes remain stationary, at an acquisition frequency of $20\,000$ Hz, the Au tip is suspended for over 200 ms after reaching the appropriate tip-substrate distance to establish molecular junctions during the retraction of the Au tip. Typical individual traces show that Au-M1 junctions switch between high and low conductance states (Figure 3a), consistent with the results presented in Figure 2d.

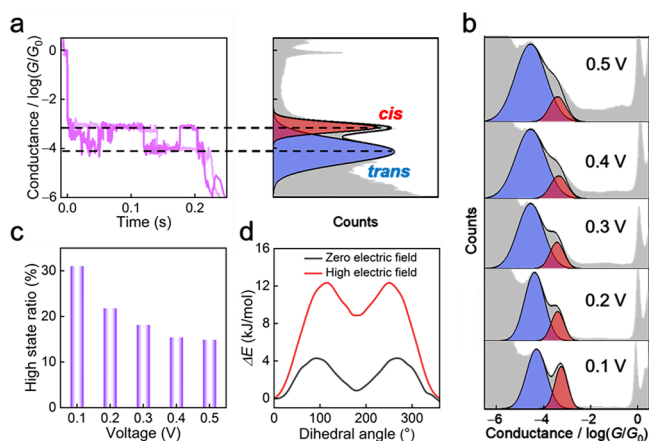


Figure 3. Transitions between high and low conductance states in M1 junctions. (a) Typical conductance–time traces (left) and 1D histogram (right). (b) 1D conductance comparison of M1 junctions over a voltage range from 0.1 to 0.5 V. (c) The high conductance ratio of M1 junctions within the voltage range of 0.1 to 0.5 V. (d) Rotational potential energy profiles of Au–M1–Au under high and zero electric fields, respectively.

By calculating the Gibbs free energy (Figure S10), it is found that the potential energy for switching between the *cis* and *trans* configurations is ~ 10 kJ/mol. This potential energy is sufficiently high to be observed at room temperature in the presence of an electric field.

Moreover, a bias-dependent test is performed to explore the impact of an electric field on the transformation between *cis* and *trans* configurations. As the bias voltage increases, the conductance of the two configurations of M1 junctions

remains relatively constant. However, the proportion of high-conductance states gradually decreases while that of low-conductance states gradually increases (Figure 3b; more 2D conductance–displacement histograms and Gaussian fittings are shown in Figure S11). Specifically, when the bias voltage increases from 0.1 to 0.5 V, the proportion of the high conductance decreases from $\sim 31.03\%$ to $\sim 14.89\%$ (Figure 3c). This indicates that the relative stability of the stereostructures can be regulated by bias voltages. Consistent results are obtained from the hover I - t bias-dependent tests (Figure S12). The STM–BJ tests are also performed on the pure solvent dodecane (Figure S13) to eliminate the influence of the solvent.

To understand the bias effect on the stereoisomerism of the Au–M1 interface, we simulate the relaxed potential energy surface (PES) of Au–M1–Au contacts concerning the rotation of the aniline groups (Figure 3d). By systematically scanning the dihedral angle of the two aniline groups in M1 across a range from 0° to 360° and optimizing each structure, we observe that the energy difference between the two stable states, characterized by dihedral angles of 0° (*trans*) and 180° (*cis*), respectively, is relatively small at zero electric field conditions (black curve). However, the potential energy of the stable 180° (*cis*) configuration becomes higher than that of 0° (*trans*) configuration under a larger electric field (red curve). This may be attributed to an increase in the molecular dipole moment under an electric field, which leads to a higher torsional potential barrier in the presence of a high electric field (Figure S14). This observation is consistent with the observed gradual decrease in the proportion of high conductance (*cis*) at high bias voltages. Considering the experimental and theoretical findings presented above, it becomes evident that the electric field can regulate the potential energy difference between different stable states of M1 junctions, thus facilitating the control of molecular transitions between high- and low-conductance states.

The universality of the interfacial stereoelectronic effect is also discussed. For example, the M2 molecule (3,4'-ethynylenebis(benzenamine)), the specific chemical formulas of M1 and M2 can be seen in Figure S15) also exhibits two anchoring modes in junctions—one on the same side (*cis*) and the other on the opposite side (*trans*)—and its electrical properties are characterized based on STM–BJ (Figure 4a). Similar to the M1 cases, the conductance–displacement traces reveal two distinct conductance plateaus corresponding to the *cis* and *trans* configurations in the solution with the M2 molecule (Figure 4b). In the 2D conductance–displacement histogram of M2 junctions, Gaussian fitting conductance peaks are observed at $\sim 0.68 \times 10^{-4} G_0$ (~ 5.24 nS) and $0.71 \times 10^{-5} G_0$ (~ 0.55 nS), as shown in Figure 4c. The flicker noise analysis of high- and low-conductance states reveals that their noise power scales are $G^{1.50}$ and $G^{1.47}$, respectively (Figure S16). These values are larger than those observed in M1 due to the meta substitution in M2.³⁶ The purple traces in Figure 4b indicate that the *cis* and *trans* configurations of Au–M2 can transition between each other, similar to Au–M1. Furthermore, the Gibbs free-energy calculations confirm the feasibility of this transformation (Figure S17). We also examined their I - V and G - V characteristics (Figure S18). The 2D I - V histogram clearly reveals the high-conductance states (Figure 4d) and low-conductance states (Figure 4e) of M2, consistent with the calculated transmission spectra for both the *cis* and *trans* configurations (see Figure 4f, as well as Figure S19). M2

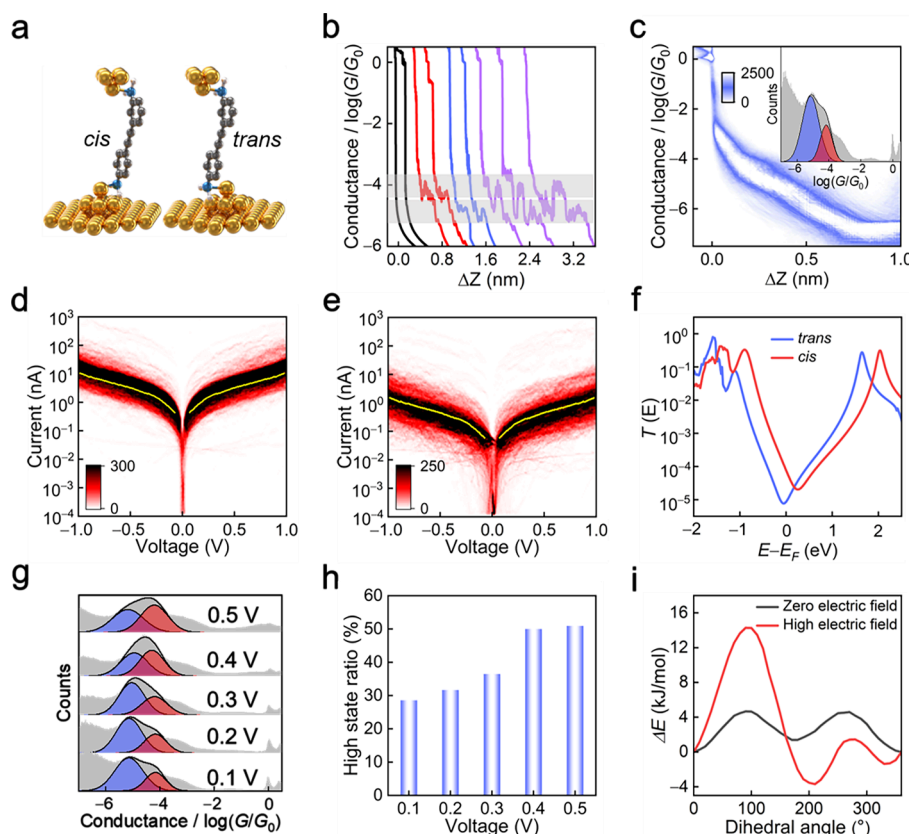


Figure 4. Single-molecule charge transport properties and electrical measurements of M2 junctions. (a) Schematic of STM–BJ measurements for a single M2 junction anchored on the same side and the opposite side. (b) Experimental conductance–displacement traces of M2 junctions at 0.1 V bias (red, blue, and purple traces) and those of Au contacts in the pure solvent (black traces). (c) 2D conductance–displacement histograms for M2 junctions. Inset shows the 1D conductance histograms of M2 junctions. (d, e) 2D I – V histograms of high- and low-conductance states of M2 junctions (see panels (d) and (e), respectively). The yellow line represents the most representative current value obtained from the Gaussian fitting. (f) Calculated transmission spectra of *cis* and *trans* conformations. (g) 1D conductance comparison of M2 junctions across a voltage range from 0.1 to 0.5 V. (h) The high conductance ratio of M2 junctions within the voltage range of 0.1 to 0.5 V. (i) Rotational potential energy profiles of Au–M2–Au under high and zero electric fields, respectively.

exhibits a HOMO distribution that is slightly less delocalized (Figure S20) and a larger energy gap (Figure S21) compared to M1. Giving that the conductance at low bias voltages is primarily influenced by HOMO (see MPSH analysis in Figure S22), it is reasonable that M2 exhibits lower conductance values for both states, compared to M1.

The impact of electric fields on the transformation between *cis* and *trans* configuration is also examined (Figure 4g and more 2D conductance–displacement histogram and Gaussian fitting shown in Figure S23). The proportion of the high conductance state in M2 junctions gradually increases from $\sim 28.57\%$ to $\sim 50.93\%$ (Figure 4h) when the bias voltage rises from 0.1 to 0.5 V. The hovering I – t bias-dependent tests of M2 yield the consistent result (Figure S24). The electric field's influence on M2 stereoisomerism is also supported by PES calculation and analysis (Figure 4i), where the *cis* configuration (180° dihedral angle) is less stable than the *trans* configuration (0° dihedral angle) at a zero electric field but becomes more stable at a high electric field. The potential energy difference between the *cis* and *trans* configurations increases under a high electric field, possibly due to the increasing dipole moment (Figure S25). This observation stands in contrast to the M1 case, highlighting the variability and case dependency of the electric field's effect on interface stereoisomerism. In addition to the Au–NH₂ anchoring-based junctions, we predict the

presence of both *cis* and *trans* configurations in other junctions, such as Au–M1 with the replacement of –NH₂ with –SH groups (Figure S26). These systems have great potential for exhibiting interfacial stereoelectronic effects.

In summary, our study highlights the ubiquitous presence of interfacial stereoelectronic effects in molecular junctions. In both M1- and M2-based molecular junctions, we observe two distinct conductance states corresponding to *cis* and *trans* configurations, which originate from same-side and opposite-side anchorings to Au, respectively. The *cis* configuration generally exhibits a higher conductance than that of the *trans* configuration. Furthermore, these two stable states can transition between each other, and their stability can be finely tuned by an applied electric field. This investigation of interfacial stereoelectronic effects has deepened the understanding of molecule–electrode interfaces, as well as provides a new perspective for the future development of practical and functional molecular nanodevices.

■ ASSOCIATED CONTENT

Supporting Information

The Supporting Information is available free of charge at <https://pubs.acs.org/doi/10.1021/acs.nanolett.4c02665>.

Experimental methods, theoretical calculations, orbital decomposition of aniline; supporting information for

M1 and M2, optimized configurations with –SH anchors (PDF)

AUTHOR INFORMATION

Corresponding Authors

Xuefeng Guo – Center of Single-Molecule Sciences, Institute of Modern Optics, Frontiers Science Center for New Organic Matter, Tianjin Key Laboratory of Micro-scale Optical Information Science and Technology, College of Electronic Information Science and Technology, Nankai University, Tianjin 300350, People's Republic of China; Beijing National Laboratory for Molecular Sciences, National Biomedical Imaging Center, College of Chemistry and Molecular Engineering, Peking University, Beijing 100871, People's Republic of China; orcid.org/0000-0001-5723-8528; Email: guoxf@pku.edu.cn

Chuancheng Jia – Center of Single-Molecule Sciences, Institute of Modern Optics, Frontiers Science Center for New Organic Matter, Tianjin Key Laboratory of Micro-scale Optical Information Science and Technology, College of Electronic Information Science and Technology, Nankai University, Tianjin 300350, People's Republic of China; Email: jiacc@nankai.edu.cn

Ping Duan – Center of Single-Molecule Sciences, Institute of Modern Optics, Frontiers Science Center for New Organic Matter, Tianjin Key Laboratory of Micro-scale Optical Information Science and Technology, College of Electronic Information Science and Technology, Nankai University, Tianjin 300350, People's Republic of China; Email: duanping@nankai.edu.cn

Authors

Xiao Wei – Center of Single-Molecule Sciences, Institute of Modern Optics, Frontiers Science Center for New Organic Matter, Tianjin Key Laboratory of Micro-scale Optical Information Science and Technology, College of Electronic Information Science and Technology, Nankai University, Tianjin 300350, People's Republic of China

Jinying Wang – Center of Single-Molecule Sciences, Institute of Modern Optics, Frontiers Science Center for New Organic Matter, Tianjin Key Laboratory of Micro-scale Optical Information Science and Technology, College of Electronic Information Science and Technology, Nankai University, Tianjin 300350, People's Republic of China

Xinyue Chang – Center of Single-Molecule Sciences, Institute of Modern Optics, Frontiers Science Center for New Organic Matter, Tianjin Key Laboratory of Micro-scale Optical Information Science and Technology, College of Electronic Information Science and Technology, Nankai University, Tianjin 300350, People's Republic of China

Suhang He – Center of Single-Molecule Sciences, Institute of Modern Optics, Frontiers Science Center for New Organic Matter, Tianjin Key Laboratory of Micro-scale Optical Information Science and Technology, College of Electronic Information Science and Technology, Nankai University, Tianjin 300350, People's Republic of China

Complete contact information is available at:

<https://pubs.acs.org/10.1021/acs.nanolett.4c02665>

Author Contributions

[†]Authors X.W. and J.W. contributed equally to this work. X.G., C.J., and P.D. conceived the idea for the paper. X.W. carried

out the experimental measurements. J.W., X.C., and S.H. built and analyzed the theoretical model and performed the quantum transport calculation. X.G., C.J., and X.W. analyzed the data and wrote the paper. All the authors discussed the results and commented on the manuscript.

Notes

The authors declare no competing financial interest.

ACKNOWLEDGMENTS

We acknowledge primary financial supports from the National Key R&D Program of China (2021YFA1200102, 2021YFA1200101, and 2022YFE0128700), the National Natural Science Foundation of China (22173050, 22150013, 21727806, and 21933001), Beijing National Laboratory for Molecular Sciences (BNLMS-CXXM-202407), and the Natural Science Foundation of Beijing (2222009).

REFERENCES

- (1) Graetzel, M.; Janssen, R. A.; Mitzi, D. B.; Sargent, E. H. Materials Interface Engineering for Solution-Processed Photovoltaics. *Nature* **2012**, *488*, 304–312.
- (2) Ren, J.; Wang, Y.; Yao, Y.; Wang, Y.; Fei, X.; Qi, P.; Lin, S.; Kaplan, D. L.; Buehler, M. J.; Ling, S. Biological Material Interfaces as Inspiration for Mechanical and Optical Material Designs. *Chem. Rev.* **2019**, *119*, 12279–12336.
- (3) Zhang, Z.; Yates, J. T., Jr Band Bending in Semiconductors: Chemical and Physical Consequences at Surfaces and Interfaces. *Chem. Rev.* **2012**, *112*, 5520–5551.
- (4) Li, P.; Chen, Y.; Wang, B.; Li, M.; Xiang, D.; Jia, C.; Guo, X. Single-Molecule Optoelectronic Devices: Physical Mechanism and Beyond. *Opto-Electron. Adv.* **2022**, *5*, No. 210094.
- (5) Zhang, Y.; Xu, L.; Sun, J.; Wu, Y.; Kan, Z.; Zhang, H.; Yang, L.; Liu, B.; Dong, B.; Bai, X.; Song, H. 24.11% High Performance Perovskite Solar Cells by Dual Interfacial Carrier Mobility Enhancement and Charge-Carrier Transport Balance. *Adv. Energy. Mater.* **2022**, *12*, No. 2201269.
- (6) Wu, K.; Chen, J.; McBride, J. R.; Lian, T. J. Efficient Hot-Electron Transfer by a Plasmon-Induced Interfacial Charge-Transfer Transition. *Science* **2015**, *349*, 632–635.
- (7) Zhang, M.; Wang, X. Two Dimensional Conjugated Polymers with Enhanced Optical Absorption and Charge Separation for Photocatalytic Hydrogen Evolution. *Energy Environ. Sci.* **2014**, *7*, 1902–1906.
- (8) Ray, B. C.; Rathore, D. Durability and Integrity Studies of Environmentally Conditioned Interfaces in Fibrous Polymeric Composites: Critical Concepts and Comments. *Adv. Colloid Interface Sci.* **2014**, *209*, 68–83.
- (9) Martins-Costa, M. T.; Ruiz-López, M. F. Electrostatics and Chemical Reactivity at the Air–Water Interface. *J. Am. Chem. Soc.* **2023**, *145*, 1400–1406.
- (10) Ren, J.; Wang, Y.; Yao, Y.; Wang, Y.; Fei, X.; Qi, P.; Lin, S.; Kaplan, D. L.; Buehler, M. J.; Ling, S. Biological Material Interfaces as Inspiration for Mechanical and Optical Material Designs. *Chem. Rev.* **2019**, *119*, 12279–12336.
- (11) Rodriguez-Emmenegger, C.; Preuss, C. M.; Yameen, B.; Pop-Georgievski, O.; Bachmann, M.; Mueller, J. O.; Bruns, M.; Goldmann, A. S.; Bastmeyer, M.; Barner-Kowollik, C. Controlled Cell Adhesion on Poly (dopamine) Interfaces Photopatterned with Non-Fouling Brushes. *Adv. Mater.* **2013**, *25*, 6123–6127.
- (12) Banks, W. A. From Blood-Brain Barrier to Blood-Brain Interface: New Opportunities for CNS Drug Delivery. *Nat. Rev. Drug. Discovery* **2016**, *15*, 275–292.
- (13) Mao, C.; Qiu, Y.; Sang, H.; Mei, H.; Zhu, A.; Shen, J.; Lin, S. Various Approaches to Modify Biomaterial Surfaces for Improving Hemocompatibility. *Adv. Colloid Interface Sci.* **2004**, *110*, 5–17.
- (14) Boyen, H. G.; Ziemann, P.; Wiedwald, U.; Ivanova, V.; Kolb, D. M.; Sakong, S.; Gross, A.; Romanyuk, A.; Büttner, M.; Oelhafen, P.

Local Density of States Effects at the Metal-Molecule Interfaces in a Molecular Device. *Nat. Mater.* **2006**, *5*, 394–399.

(15) Gaita-Ariño, A.; Luis, F.; Hill, S.; Coronado, E. Molecular Spins for Quantum Computation. *Nat. Chem.* **2019**, *11*, 301–309.

(16) Jia, C.; Guo, X. Molecule-Electrode Interfaces in Molecular Electronic Devices. *Chem. Soc. Rev.* **2013**, *42*, 5642–5660.

(17) Inkpen, M. S.; Liu, Z. F.; Li, H.; Campos, L. M.; Neaton, J. B.; Venkataraman, L. Non-Chemisorbed Gold-Sulfur Binding Prevails in Self-Assembled Monolayers. *Nat. Chem.* **2019**, *11*, 351–358.

(18) Schwarz, F.; Kastlunger, G.; Lissel, F.; Riel, H.; Venkatesan, K.; Berke, H.; Stadler, R.; Lörtscher, E. High-Conductive Organometallic Molecular Wires with Delocalized Electron Systems Strongly Coupled to Metal Electrodes. *Nano Lett.* **2014**, *14*, 5932–5940.

(19) Li, J.; Hou, S.; Yao, Y.; Zhang, C.; Wu, Q.; Wang, H.; Zhang, H.; Liu, X.; Tang, C.; Wei, M.; et al. Room-Temperature Logic-in-Memory Operations in Single-Metallofullerene Devices. *Nat. Mater.* **2022**, *21*, 917–923.

(20) Zang, Y.; Pinkard, A.; Liu, Z.; Neaton, J. B.; Steigerwald, M. L.; Roy, X.; Venkataraman, L. Electronically Transparent Au–N Bonds for Molecular Junctions. *J. Am. Chem. Soc.* **2017**, *139*, 14845–14848.

(21) Reed, M. A.; Zhou, C.; Muller, C.; Burgin, T.; Tour, J. Conductance of a Molecular Junction. *Science* **1997**, *278*, 252–254.

(22) Zhou, P.; Zheng, J.; Han, T.; Chen, L.; Cao, W.; Zhu, Y.; Zhou, D.; Li, R.; Tian, Y.; Liu, Z.; Liu, J.; Hong, W. Electrostatic Gating of Single-Molecule Junctions Based on the STM-BJ Technique. *Nanoscale* **2021**, *13*, 7600–7605.

(23) Hadeed, F.; Durkan, C. Controlled Fabrication of 1–2 nm Nanogaps by Electromigration in Gold and Gold-Palladium Nanowires. *Appl. Phys. Lett.* **2007**, *91*, No. 123120.

(24) Baumans, X. D. A.; Cerbu, D.; Adami, O.-A.; Zharinov, V. S.; Verellen, N.; Papari, G.; Scheerder, J. E.; Zhang, G.; Moshchalkov, V. V.; Silhanek, A. V.; Van de Vondel, J. Thermal and Quantum Depletion of Superconductivity in Narrow Junctions Created by Controlled Electromigration. *Nat. Commun.* **2016**, *7*, 10560.

(25) Guo, X.; Small, J. P.; Klare, J. E.; Wang, Y.; Purewal, M. S.; Tam, I. W.; Hong, B.; Caldwell, R.; Huang, L.; O'Brien, S.; et al. Covalently Bridging Gaps in Single-Walled Carbon Nanotubes with Conducting Molecules. *Science* **2006**, *311*, 356–359.

(26) Jia, C.; Ma, B.; Xin, N.; Guo, X. Carbon Electrode-Molecule Junctions: A Reliable Platform for Molecular Electronics. *Acc. Chem. Res.* **2015**, *48*, 2565–2575.

(27) Xie, X.; Li, P.; Xu, Y.; Zhou, L.; Yan, Y.; Xie, L.; Jia, C.; Guo, X. Single-Molecule Junction: A Reliable Platform for Monitoring Molecular Physical and Chemical Processes. *ACS Nano* **2022**, *16*, 3476–3505.

(28) Häkkinen, H. The Gold-Sulfur Interface at the Nanoscale. *Nat. Chem.* **2012**, *4*, 443–455.

(29) Elf, J.; Li, G.; Xie, X. Probing Transcription Factor Dynamics at the Single-Molecule Level in a Living Cell. *Science* **2007**, *316*, 1191–1194.

(30) Zang, Y.; Fung, E.; Fu, T.; Ray, S.; Garner, M. H.; Borges, A.; Steigerwald, M. L.; Patil, S.; Solomon, G.; Venkataraman, L. Voltage-Induced Single-Molecule Junction Planarization. *Nano Lett.* **2021**, *21*, 673–679.

(31) Su, T. A.; Li, H.; Steigerwald, M. L.; Venkataraman, L.; Nuckolls, C. Stereoelectronic Switching in Single-Molecule Junctions. *Nat. Chem.* **2015**, *7*, 215–220.

(32) Xin, N.; Wang, J.; Jia, C.; Liu, Z.; Zhang, X.; Yu, C.; Li, M.; Wang, S.; Gong, Y.; Sun, H.; et al. Stereoelectronic Effect-Induced Conductance Switching in Aromatic Chain Single-Molecule Junctions. *Nano Lett.* **2017**, *17*, 856–861.

(33) Yang, C.; Shen, P.; Ou, Q.; Peng, Q.; Zhou, S.; Li, J.; Liu, Z.; Zhao, Z.; Qin, A.; Shuai, Z.; Tang, B. Z.; Guo, X. Complete Deciphering of the Dynamic Stereostructures of a Single Aggregation-Induced Emission Molecule. *Matter* **2022**, *5*, 1224–1234.

(34) Reid, R. C.; Yau, M. K.; Singh, R.; Lim, J.; Fairlie, D. P. Stereoelectronic Effects Dictate Molecular Conformation and Biological Function of Heterocyclic Amides. *J. Am. Chem. Soc.* **2014**, *136*, 11914–11917.

(35) Meng, L.; Xin, N.; Wang, J.; Xu, J.; Ren, S.; Yan, Z.; Zhang, M.; Shen, C.; Zhang, G.; Guo, X.; Meng, S. Atomically Precise Engineering of Single-Molecule Stereoelectronic Effect. *Angew. Chem., Int. Ed.* **2021**, *60*, 12274–12278.

(36) Adak, O.; Rosenthal, E.; Meisner, J.; Andrade, E. F.; Pasupathy, A. N.; Nuckolls, C.; Hybertsen, M. S.; Venkataraman, L. Flicker Noise as a Probe of Electronic Interaction at Metal–Single Molecule Interfaces. *Nano Lett.* **2015**, *15*, 4143–4149.

(37) Tang, Y.; Zhou, Y.; Zhou, D.; Chen, Y.; Xiao, Z.; Shi, J.; Liu, J.; Hong, W. Electric Field-Induced Assembly in Single-Stacking Terphenyl Junctions. *J. Am. Chem. Soc.* **2020**, *142*, 19101–19109.

(38) Moreno-García, P.; Gulcur, M.; Manrique, D. Z.; Pope, T.; Hong, W.; Kaliginedi, V.; Huang, C.; Batsanov, A. S.; Bryce, M. R.; Lambert, C.; Wandlowski, T. Single-Molecule Conductance of Functionalized Oligoynes: Length Dependence and Junction Evolution. *J. Am. Chem. Soc.* **2013**, *135*, 12228–12240.

(39) Hong, W.; Manrique, D. Z.; Moreno-García, P.; Gulcur, M.; Mishchenko, A.; Lambert, C. J.; Bryce, M. R.; Wandlowski, T. Single Molecule Conductance of Tolanes: Experimental and Theoretical Study on the Junction Evolution Dependent on the Anchoring Group. *J. Am. Chem. Soc.* **2012**, *134*, 2292–2304.

(40) Hybertsen, M. S.; Venkataraman, L.; Klare, J. E.; Whalley, A. C.; Steigerwald, M. L.; Nuckolls, C. Amine-Linked Single-Molecule Circuits: Systematic Trends Across Molecular Families. *J. Phys.: Condens. Matter* **2008**, *20*, No. 374115.